Proceedings of
ASME TURBOEXPO 2000
May 8-11, 2000, Munich Germany

2000-GT-554

Submitted for presentation at the International Gas Turbine Institute meeting of the
American Society of Mechanical Engineers, May 8-12, 2000

DEVELOPMENT OF DYNAMIC MODELING TOOLS FOR SOLID OXIDE AND MOLTEN CARBONATE HYBRID FUEL CELL GAS TURBINE SYSTEMS

Randall S. Gemmen, Eric Liese
National Energy Technology Laboratory, Morgantown, WV

Jose G. Rivera, Faryar Jabbari and Jacob Brouwer
National Fuel Cell Research Center, Univ. of California, Irvine, CA

ABSTRACT

This paper describes some generic solid oxide and molten carbonate hybrid fuel cell gas turbine systems and dynamic modeling tools that are being developed to simulate the performance of these and other hybrid fuel cell systems. The generic hybrid systems are presented to introduce issues and technical development challenges that hybrid fuel cell gas turbine systems must address and to provide a platform for the development of the dynamic modeling tools. The present goals are to develop dynamic models for the basic components of solid oxide and molten carbonate fuel cell gas turbine hybrids, ensure their reliability, and obtain a basic understanding of their performance prior to integration into a complete hybrid system model. Preliminary results for molten carbonate and solid oxide fuel cell types are presented. These results provide understanding of some of the operational characteristics of fuel cells, and indicate the complexity of the dynamic response of fuel cell hybrid components. For the fuel cell models, generic planar designs are analyzed showing voltage and current behavior following step changes in load resistance and steady state performance curves. The results provide confidence in each of the model's reliability, enabling them to be integrated for hybrid system simulation. Results from the integrated simulations will provide guidance on future hybrid technology development needs.

NOMENCLATURE

A	Area at the inlet/outlet of the control volume [m^2]
P	Pressure at the inlet/outlet of the control volume [Pa]
$P_{CH4,H2O,H2,CO2}$	Partial pressures
C_i	Molar concentration of species i [kgmole/m^3]
dt	Time step differential [sec]
E	Energy storage [kJ/hr] control volume [joule/kg] for fuel cell
F	Faraday Constant
F_s	Control volume surface frictional force [N]
G	Gibbs free energy
ΔH_{H2O}	Heat of H_2O formation [kJ/kgmol]
i	Current Density
i_o	Exchange Current Density
i_L	Diffusion Limiting Current Density
N_i	Molar flow rate of specie i (in/out of control volume) [kgmole/s]
n	Number of participating electrons per H2 molecule
Q_s	Net boundary heat addition [W].
R_i	Molar source of specie i [kgmole/s]
R_u	Universal gas constant

T	Temperature [K]
Ut	Utilization
r	Reaction rate [kgmol CH_4/hr/m^3 catalyst]
V	Finite control volume [m^3]
v	Velocity [m/s]
w	mass flow [kg/s]
y	Mole fraction
Greek	
α	Electrochemical transfer coefficient
ρ	Density [kg/m^3]

INTRODUCTION

Fuel cells have the potential to play a significant role in meeting near- and medium-term requirements for efficient and environmentally responsible power generation. Hybrid fuel cell and gas turbine technology is potentially superior to other power generation technologies due to its high efficiency (70 to 80 percent LHV) and low emissions (less than 3 parts per million NOx and CO). However, to advance the technology to the commercial level requires a better understanding of how gas turbines and fuel cells should be integrated and how they will behave when fused into a single hybrid system.

The combination of a fuel cell and a gas turbine is a natural evolution in the quest for improved generation efficiency with low emissions. Integrated hybrid cycles exhibit synergies not present in typical combined cycles with fuel-to-electricity efficiencies higher than either the fuel cell or gas turbine alone and costs for a given efficiency lower than either alone.

This paper begins with a description of some basic operational characteristics of two generic hybrid systems. The paper continues with a presentation of the fuel cell submodels necessary for eventual integration into a complete hybrid model. Two commercial transient analysis software packages, ProTRAX, which is widely employed for power generation applications, and SABER, which is widely used for electronics and automotive applications, are used for model development and integration. These analysis packages contain many process elements required for typical power generation applications; however, at this time the user is required to supply specialized submodels for the fuel cells and other non-standard hybrid components.

GENERIC HYBRID CYCLES

Hybrid cycles are myriad. Typical fuel cell gas turbine configurations include topping cycles (where the fuel cell replaces a combustor and generator and the gas turbine is the balance of plant) and bottoming cycles (where the fuel cell uses the gas turbine exhaust as an air supply and the fuel cell is the balance of plant). Depending upon the cycle, theoretical fuel-to-electricity efficiencies are between 80 and 90 percent with achievable efficiencies ranging from 58 percent for small hybrids to 72 percent for large hybrids and up to 80 percent for large hybrid combined cycle systems.

In general, topping cycles lead to the highest efficiency systems with high oxygen concentration at the cathode, fewer cells required in the fuel cell stack as compared to low pressure systems and higher power density. Bottoming cycles perform well depending upon the fuel cell type and are simple to integrate, easy to start and simple to control. To achieve high efficiencies, most of the electricity of a hybrid system is produced in the fuel cell (typically between 70 and 80 percent).

Generic Solid Oxide Hybrid

A generic solid oxide fuel cell gas turbine engine hybrid system is presented in Figure 1. The selection of a recuperated gas turbine rather than simple cycle machine is largely driven by the design and construction of the solid oxide fuel cell (SOFC). If it is possible to recirculate part of the anode exhaust flow (slightly fuel rich to avoid any oxygen content) to the fuel reformer, then no steam need be raised in the exhaust thus eliminating the need for a boiler. When anode flows are used to provide steam, the reformer is often integrated into the SOFC proper. With these SOFC systems it is advantageous to use a recuperated gas turbine to increase fuel cell efficiency, since both inlet air temperature and air pressure is increased. The pressure ratio for recuperated engines (3:1 to 8:1) is reasonable for use with a SOFC. The high inlet air temperatures also minimize temperature gradients through the fuel cell thereby prolonging its life.

Generic Molten Carbonate Hybrid

A generic molten carbonate fuel cell gas turbine engine hybrid system is presented in Figure 2. The simplest type of hybrid system can be called a bottoming cycle or low pressure hybrid cycle. There are two basic versions of this arrangement; one uses a fired gas turbine and the other an indirectly heated gas turbine where the required thermal energy is extracted by heat exchange from the fuel cell exhaust.

The fired version simply uses the fuel cell component as a true bottoming cycle with the gas turbine exhaust supplying the air to the fuel cell. This is the generic hybrid molten carbonate cycle selected for presentation in Figure 2. Both the gas turbine and the fuel cell generate electrical power in this arrangement.

Although both the SOFC and the MCFC can be employed in this form of bottoming cycle, the MCFC is much better suited because it can use the carbon dioxide and the oxygen in the turbine's exhaust without efficiency penalties. In fact the MCFC requires carbon dioxide to be added to the inlet air stream to allow the production of the carbonate ion. Thus the MCFC accrues an advantage in this arrangement

over the SOFC in the elimination of the high temperature blower used to take high temperature carbon dioxide rich exhaust and add it to the inlet air stream, reducing costs and improving overall efficiency.

Modeling Needs

It is clear that the operational complexity for hybrid systems is relatively high, which indicates that to reduce technical development risks, new engineering tools will be needed. Fortunately, as evidenced in the following sections, our basic understanding of the dynamic characteristics of major hybrid components (reformer and fuel cell) is also fairly high. When fully integrated into models representing hybrid systems, these modeling tools will enable greater insight into the operational characteristics for hybrid systems, and provide opportunities for resolving any identified problems.

MOLTEN CARBONATE FUEL CELL MODEL

This analysis is based on a $100cm^2$, single, co-flow, planar fuel cell. The configuration of the fuel cell is shown in Figure 3. The analysis considers the behavior of a single unit cell located within an infinite series of cells undergoing the same dynamics; hence, the overall thickness of the unit cell (*separator plate* to *separator plate*) is a *symmetry length*, and for computational efficiency, the only length that needs to be resolved. Finally, because the present analysis considers the electrochemistry as quasi-steady and assumes a low Biot number for the solid/gas heat transfer, only the bulk (transverse-lumped) behavior of the separator plate and cell components need to be modeled. Here, the term *cell* is used to describe the lumped anode and cathode electrodes together with the electrolyte material.

Fuel cell parameters and operating conditions employed for the present analysis are shown in Table 1. The operating conditions are those at the initial steady state condition. The values of the cell parameters and operating conditions do not represent any particular cell currently under development—as known by the authors.

Assumptions

1. One-dimensional behavior along the streamwise direction.
2. Lumped temperature for the cell.
3. Heat transfer is by convection. Radiation is ignored at this time, but in general can be important.
4. There is no carbon deposition.
5. Although in reality some rates in the overall electrochemical process can occur on the order of 10^{-3} s, Andrew (1966), the electrochemistry is assumed quasi-steady as described by the Butler-Volmer equation.
6. No gas phase reactions occur.
7. Diffusional losses are based on a constant transport coefficient and diffusion layer--i.e., fully developed flow exists.
8. Cell ohmic resistance is fixed, but in general is a function of temperature.
9. Anode electrochemical activation overpotential is negligible, Srinivasan et al. (1991).
10. The fuel cell has 100 percent current efficiency--all reactants generate their ideal number of electrons. This is characteristic of a hydrogen fuel cell that avoids such side reactions as reduction of metal oxides, Liebhafsky and Cairns (1968).
11. Heat transfer coefficients are calculated by assuming anode gas as H_2 and cathode gas as N_2.
12. Carbon dioxide adsorption is not included in the analysis as having an effect on heat transfer.
13. Pressure at the anode and cathode are equal.

Table 1. Unit Cell Data and Operating Conditions for the MCFC Dynamic Model

Parameter	Unit	Value	
Load Resistance	ohm	0.0807	
Anode Specification			
Inlet Temperature	K	900	
Inlet Flow Rate	mol/s	0.0005455	
Inlet H_2 Mole Fraction		0.950	
Inlet H_2O Mole Fraction		0.050	
Cathode Specification			
Inlet Temperature	K	900	
Inlet Flow Rate	mol/s	0.0028164	
Inlet O_2 Mole Fraction		0.126	
Inlet N_2 Mole Fraction		0.690	
Inlet CO_2 Mole Fraction		0.184	
Exchange Current Density	amp/m^2	4	
Transfer Coefficient		0.5	
Cell Specification			
Thickness		m	0.001
Heat Capacity	J/kg-K	800	
Density	kg/m^3	1500	
Net Resistance	ohm-m^2	0.000034	
Separator Specification			
Thickness		m	0.002
Heat Capacity	J/kg-K	400	
Density	kg/m^3	8000	

Gas Phase Equations

For both the anode and cathode gases, the following conservation equations are employed at each finite control volume, Lucas et al. (1999). For species conservation:

$$V\frac{dC_i}{dt} = N_{i_{inlet}} - N_{i_{outlet}} + R_i \quad (1)$$

For momentum conservation:

$$V\frac{d(\rho\bar{v})}{dt} = P_{inlet}\,A_{inlet} - P_{outlet}\,A_{outlet} - F_s \quad (2)$$

For energy conservation:

$$V\frac{d(\rho E)}{dt} = \Sigma\, w_{inlet}\,E_{inlet} - \Sigma\, w_{outlet}\,E_{outlet} + Q_s + P' \quad (3)$$

The molar source of species i, R_i, arises from the electrochemistry occurring at the surface of the gas phase control volume. These sources are directly related to the current flow according to the number of electrons carried by the ions created in the electrochemical process. For the present analysis, two electrons are carried by each oxygen ion which consumes two hydrogen atoms at the anode surface.

For all control volumes but at the exit, E is the sum of internal energy and kinetic energy. For the exit control volume we assume pressure fluctuations are zero (constant pressure boundary condition), and the enthalpy is used in place of the internal energy. In Equation (3), a summation over all inlet and outlet energy flows arises due to species transport by bulk convection, and diffusion at the electrode surfaces.

Solid Phase Energy Equation

For both the cell and separator plate, an energy equation similar to Equation (3) arises, but the flow energy terms for the separator plate will be zero. Equation (4) expresses the heat generated by the production of H_2O.

$$Q_{gen} = \frac{i\Delta H_{H2O}}{nF} \tag{4}$$

Cell Voltage and Loss Mechanisms

The quasi-steady electrochemistry is modeled by assuming ideal behavior and then accounting for various loss mechanisms. The reversible potential of the fuel cell at standard state conditions is given by:

$$E^{\circ} = -\frac{\Delta G}{nF} \tag{5}$$

The general form of the Nernst Equation for an MCFC is:

$$E = E^{\circ} + \frac{R_u T}{nF} \ln\left[\frac{[y_{H2}][y_{O2}]^{1/2}[y_{CO2,c}]P^{1/2}}{[y_{H2O}][y_{CO2,a}]}\right] \tag{6}$$

where $P_c = P_a = P$ is assumed.

The main losses (i.e., referred to as *overpotentials* by electrochemists) are due to electrical resistance, concentration, and activation, Hirschenhofer et al. (1994). For the present work, they are given here as, respectively:

$$L_R = iR_{net} \tag{7}$$

$$L_C = -\frac{R_u T}{nF} \ln(1 - i/i_L) \tag{8}$$

$$L_A = \frac{R_u T}{n\alpha F} \ln(i/i_o) \tag{9}$$

where i is the local current density through the control volume. i_L is the diffusion limiting current density, which for the present work is limited by the cathode oxygen transport at near 4000 amp/m^2.
So the corrected cell voltage becomes:

$$E_{cor} = E - L_R - L_C - L_A \tag{10}$$

which must equal the voltage across the load resistance.

Numeric Representation and Solution Technique

The one-dimensional problem outlined above was modeled using 5 finite difference control volumes along the streamwise direction for each of the four major components: anode gas, cathode gas, cell, and separator plate. In order to solve for inlet flow rates of anode and cathode, the following parameters need to be chosen.

1) Hydrogen and carbon dioxide utilizations.
2) Fuel cell load current.
3) Anode and cathode gas compositions.

$$N_{i,inlet} = \frac{N_{i,consumed}}{Ut_i} \tag{11}$$

For the present analysis, the flow rates for the components can be inferred from the data in Table 1.

A load perturbation is applied at 1500 seconds following a steady state condition. To determine the current density profile, an iterative approach at each time step is required to ensure that the actual cell voltage matches the voltage achieved across the load. Finally, the present objective is to examine the short time scale (10^0 s) behavior of the fuel cell, and an explicit time marching technique was employed. Future work will incorporate balance of plant of a specific MCFC test stand. The goal is to use the data acquired by this 100-cm2 MCFC test stand and validate the results of this dynamic model.

Molten Carbonate Fuel Cell Model Results

One perturbation mechanism typical of power generation applications was selected: a load change. For the load perturbation, the load resistance is raised by 20 percent to simulate the effect of a drop in fuel cell current demand.

Increase in Load Resistance

The effect of increased resistance on the cell output voltage is shown in Figure 4a. The output voltage transient exhibits a relatively fast and large increase (time constant of order 10^{-2} s), followed by a slower and smaller increase (time constant of order 10^0 s). The first transient is due to the fast readjustment of the electrochemistry, and the second is due to the combined effects of material residence and thermal response times. The initial voltage increase is from 0.800 to 0.831 volts, or about a 3.9 percent increase. The final steady state voltage is approximately 0.839 volts, for an overall voltage increase of about 4.9 percent.

Figure 4b shows the distribution in current density across the fuel cell, while Figure 4c is the distribution of losses across the different loss mechanisms (each normalized by the total loss). As Figure 4b shows, the increased load resistance results in a 13 percent decrease in total current flow. As is clearly evident in the model equations, a decrease in current decreases the losses for the fuel cell. The results in Figure 4c shows a redistribution of the total losses between the various loss mechanisms due to the resistance increase. In particular, the cathode activation provides a relatively higher proportion of the total loss, while the ohmic losses have been decreased. Finally, as for the load voltage behavior, all the parameters shown in the latter two figures exhibit an initially fast transient followed by a second slower transient.

Figures 4d and 4e show the results for the hydrogen mole fraction in the anode gas stream and the anode gas temperature, respectively. In contrast to the electrochemical behavior, these two figures show only one relatively long transient, which is on the same order as the second transient noted previously for the electrochemistry (10^0 s). As is seen in Figure 4d, the upstream nodes have a relatively small H_2 response, while the downstream nodes show a relatively large H_2 response. As the consumption of H_2 is directly related to the current flow, the results shown in Figure 4d can be viewed as a time-wise cumulative representation of the perturbation in current density shown in Figure 4b. Regarding future hybrid developments, such large changes in fuel utilization need to be carefully considered in the design of any downstream combustor which may release this energy as thermal energy prior to entering a heat engine. Finally, since less fuel is being converted, and since conversion occurs at a higher efficiency, there should be less heat generated within the system resulting in a decrease in temperature. This is confirmed in the temperature results shown in Figure 4e.

SOLID OXIDE FUEL CELL MODEL

Details of a model for a generic bi-polar, co-flow, planar fuel cell were described in Liese et al. (1999). Figure 5 shows the basic geometry of the system under study. Again, the analysis considers the behavior of a single unit cell located within an infinite series of cells undergoing the same dynamics. In this initial work, basic dynamic behavior of a fuel cell undergoing load and input flow changes was presented. Radiation was ignored, temperature independent *resistances* and *exchange current densities* for the cell were assumed, and internal reforming was unavailable. Progress has been made so that the assumptions of constant resistances and exchange current density are no longer employed. In addition, the model is now capable of radiation heat transport and internal reforming. This paper continues the discussion of fuel cell model development with results that include the effect of temperature dependant resistances and exchange current density. Results from the addition of the two latter features, radiation and reforming, will be presented in a separate paper.

Since the focus of this work is the study of dynamics occurring within a hybrid system, it is important that each component in the hybrid model be as computationally efficient as possible while still providing accurate results. Following a discussion of the aforementioned refinements to the model, the work presented here shows results of an investigation to determine the minimum number of computational nodes required to ensure reasonable results. More importantly, the investigation shows what aspects of the fuel cell operation drive these requirements.

Also shown in this paper are results from evaluation tests performed to ensure that the model correctly describes the basic steady-state operational features of a typical fuel cell. These tests provided V-I (voltage-current) curves under different fuel-flow input conditions. Such results can be compared to standard test data used to characterize a given fuel cell's performance. Also presented in this paper are "lite-off" and "extinction" curves that show the temperature sensitivity of the fuel cell's operation, and how a fuel cell exhibits thermal hysteresis similar to most combustion systems.

Model Refinements—Temperature Dependant Properties

Solid oxide materials used for the electrolyte, electrodes, and interconnects or separator plates have strong temperature dependant resistivities. The resistances depend not only on the basic materials used, but also on how the cell is manufactured. To describe the temperature dependant resistances for these cell components, the following equation is used:

$$R = Ae^{(E/T)} \tag{12}$$

where R is the resistivity of the material and T is the absolute temperature of the material. Table 2 shows the values of A and E used for the various components, and their assumed effective thickness through which current flows.

By adding up the resistances for all components, the total cell resistance for each computational node can be determined which is used to evaluate the ohmic loss inside the cell.

Table 2. Cell and Separator Component Data, 'A' and 'E' values from Bessette (1994)

	Fractional Thickness of Cell [1]	Pre-Exponential Factor 'A' [ohm-cm]	Exponential Factor 'E' [K]
Anode Electrode	0.42	0.00298	-1392.0
Cathode Electrode	0.5	0.008144	600.0
Electrolyte	0.03	0.00294	10350.0
Separator Plate	0.05	0.1256	4689.0

For the exchange current density, which is used to describe the electrochemical losses, a linear temperature dependency is assumed following the work of Bessette (1994):

$$i_o = B + M \cdot T \qquad (13)$$

where i_o is the exchange current density, and T is the absolute temperature. The values of the coefficients 'B' and 'M' can be found in Table 3. The exchange current density depends not only on the basic material used, but also on how the cell is manufactured.

Table 3. Unit Cell Data and Operating Conditions

Cell Voltage	V	0.7
Anode Specification		
Inlet Temperature	Deg. C	800
Inlet Pressure	Pa	101050
Exit Pressure	Pa	101000
Inlet H_2 Mole Fraction	[1]	0.7272
Inlet H_2O Mole Fraction	[1]	0.0910
Inlet CO_2 Mole Fraction	[1]	0.1818
Cathode Specification		
Inlet Temperature	Deg. C	600
Inlet Pressure	Pa	101050
Exit Pressure	Pa	101000
Inlet O_2 Mole Fraction	[1]	0.21
Inlet N_2 Mole Fraction	[1]	0.79
Exchange Current Density 'M'	amp/K-m^2	15.0
Exchange Current Density 'B'	amp/m^2	-13595.0
Transfer Coefficient	[1]	0.5
Cell Specification		
Thickness	m	0.00318
Heat Capacity	J/kg-K	800
Density	kg/m^3	1500
Separator Specification		
Thickness	m	0.002
Heat Capacity	J/kg-K	400

Node-Number Analysis

Except as noted, the fuel cell parameters and operating conditions employed for the node-number sensitivity analysis are as shown in Table 3. The anode (fuel) gas inlet conditions correspond to a fully reformed methane-steam mixture ($H_2O/CH_4 = 2.5$). As in the previous work (Liese et al., 1999), these values are intended to be generic, and do not apply to any particular fuel cell developer's technology.

Results from this analysis are shown in Figures 6 and 7. Figure 6 shows how, for three different cathode gas (air) supply temperatures, the cell temperature profile changes with the number of nodes employed. For simple linear systems, the use of one node could be expected to provide the same "average" cell temperature as when using more than one node. It is easily seen from these results, however, that (depending on operating condition) there is a significant variation in the average predicted temperature when using different number of nodes. The variation is particularly significant for the 600 deg. C case shown--as the number of nodes increase, significantly different temperature profiles result. For any of the cases shown, depending on the accuracy needed, as many as eight or more nodes are required in order to best resolve the temperature profile. Because the temperature profile is not a simple linear one (and likewise for the other parameters), and because many of the critical processes occurring in a fuel cell are non-linear, it is unlikely that a single node (lumped model) for a fuel cell model can adequately predict the general behavior of a fuel cell.

These results are further supported by Figure 7, which shows how the predicted fuel utilization and air utilization change as the number of nodes increase. The reason that the air and fuel curves for the same case may have different shapes as the nodes increase is that both the air and fuel flow rates can vary independently as the system of equations are solved for the specified overall pressure drops across both anode and cathode channels. Again, depending on the desired accuracy, approximately ten or more nodes are required.

Finally, in reference to hybrid systems that employ un-cooled turbine technology, it is seen that the 700 deg. C cathode gas results provide the highest temperature fuel cell output acceptable to most un-cooled turbines available today.

Model Evaluation

The steady-state performance of a generic fuel cell was analyzed to ensure that the overall model could predict the general behavior of a real fuel cell, Hirschenhofer et al. (1994). This aspect of the work evaluates the model to assure consistency with observed fuel cell performance. (The model will be *validated* against data, once the relevant data has been produced via experiments.) Model evaluation results are provided in Figure 8, which shows several voltage vs. current curves for a given fuel cell. Except as noted in the figure, all fuel cell parameters are the same as in Tables 2 and 3. The only control variable changed from case-to-case is the fuel flow rate.

As can be seen from Figure 8, the anode gas flow rate can significantly affect the fuel cell's performance. At the Base Case fuel flow rate, the system exhibits a linear drop in voltage as current increases up to 4000 A (400 mA/cm^2) where it shows a sharp drop in voltage. If the fuel flow rate is decreased, the overall curve falls along the y-axis, and the sudden voltage drop occurs at a lower current. For fuel flow rates higher than the base case, the sudden drop in voltage becomes less evident.

The behavior show in Figure 8 indicates that for these conditions the reduction in cell voltage with current results mainly from ohmic losses. The sudden drop in voltage for several of the curves results due to the high consumption (utilization) of fuel. Such a high consumption reduces the reactant concentration at the exit of the fuel cell, and as a result, lowers the ideal (i.e., Nernst) voltage. In summary, the behavior predicted by the model is found to be representative of data available in the literature, Hirschenhofer et al. (1994), and Kordesch and Simader (1996), and provides support for its use in our hybrid modeling activity.

More Aspects of SOFC Operation

General discussions of hybrid systems have already suggested how fuel cells behave analogous to combustion systems in that they provide an increase in gas stream thermal energy. It is shown here that fuel cells also exhibit another behavior similar to that of combustion systems—namely, "lite-off" and "extinction" hysteresis. To the authors' understandings, such a perspective of fuel cell operation has not been previously described within the literature.

Figure 9 shows the behavior of a fuel cell undergoing "lite-off" and "extinction" as the load demand changes. The parameters used in the analysis are again the same as in Tables 2 and 3, except that the cathode supply temperature is now 500 deg. C (a condition possible at startup of the hybrid system). This analysis does not necessarily describe a preferred, or optimal, lite-off strategy for a real fuel cell, but rather examines the behavior of this fuel cell model undergoing the prescribed changes in load (voltage and current).

As can be seen in Figure 9, when a fuel cell begins cold with a temperature of 760 K, very little current flows and the cell voltage is near 0.6 V. As the request for current increases, the voltage drops and the cell temperature gradually rises. As the current is further increased, the system reaches a condition where, for the same voltage, there can be a sudden increase in electric current and cell temperature which at this time we describe as a "lite-off". This sudden increase in current is possible due to the strong decrease in cell resistance as the cell temperature rises. The strong increase in cell temperature is itself supported by the strong rise in current due to the dissipation within the fuel cell as fuel is converted into electricity.

With the system now "lit", if current demand is now decreased, the cell temperature gradually decreases, and the voltage increases, but both now along a different trajectory. Once the cell voltage reaches approximately 0.42 V, there can be a strong drop in temperature and current, and the fuel cell is "extinguished". Hence, we see that a fuel cell can exhibit additional "combustor-like" behavior—the internal reactions occurring in both technologies are self-supported by a thermal energy release, thereby providing a hysteresis it its operation.

An important result from this part of the analysis is the understanding that these systems can exhibit non-monotonic V-I characteristics. A point not commonly made in the literature.

SUMMARY

Models have been generated and studied for two potential hybrid system components, a molten carbonate and solid oxide fuel cell. Each model shows behavior that is consistent with previously reported fuel cell performance, which engenders confidence in their future application to hybrid system studies. In addition, the present results begin to highlight some of the features that need to be considered in the future design of hybrid systems; e.g., fuel cell transient and steady state operating characteristics, combustor design and necessary response times for control elements. The results also continue to demonstrate the complexity of the fuel cell component behavior, which emphasizes the need for such simulation capability.

REFERENCES

Andrew, M.R., "Chapter 4, Kinetic Effects--Part 2," in *An Introduction to Fuel Cells*, ed. K.R. Williams, Elsevier Publishing Company, New York, (1966).

Bessette, N.F., "Modeling and Simulation for Solid Oxide Fuel Cell Power Systems," Ph.D. Thesis (1994).

Cebeci, T., and P. Bradshaw, *Physical and Computational aspects of Convective Heat Transfer*, Springer-Verlay, New York (1988).

He, W., "Dynamic Response of a Reformer for Molten Carbonate Fuel Cell Power-Generation Systems," *Fuel Processing Technology*, **53**, 99-113 (1997).

Hirschenhofer, J.H., D.B. Stauffer, and R.R. Engleman, "Fuel Cells—A Handbook (Revision 3)," DOE/METC-94/1006 (1994).

Kordesch, K. and G. Simader *Fuel Cells and Their Applications*, VCH Verlagsgesellschaft, New York (1996).

Kortbeek, P. J., de Ruijter, J. A. F., van der Laag, P. C., Barten, H., "A Dynamic Simulator for a 250 kW class ER-MCFC system," Journal of Power Sources, Vol. 71, pp. 278-780 (1998).

Liebhafsky, H.A. and E.J. Cairns, "Fuel Cells and Fuel Batteries--A Guide to Their Research and Development," p. 85, John Wiley & Sons, New York, (1968).

Liese, E.A., R.S. Gemmen, F. Jabbari, and J. Brouwer (1999). "Technical Development Issues and Dynamic Modeling of Gas Turbine and Fuel Cell Hybrid Systems," to be published in Journal of Engineering for Gas Turbines and Power.

Lukas, M.D., K.Y. Lee, and H. Ghezel-Ayagh, "Development of a Stack Simulation Model for Control Study on Direct Reforming Molten Carbonate Fuel Cell Power Plant," Submitted to IEEE Power Engineering Society, 1999 Winter Meeting, New York, NY.

Srinivasan, S. A.V. Omourtag, A. Parthasarathy, D.J. Manko, and A.J. Appleby, "High Energy Efficiency and High Power Density Proton Exchange Membrane Fuel Cells -- Elecrode Kinetics and Mass Transport," J. Power Sources, **36**, pp. 299-320 (1991).

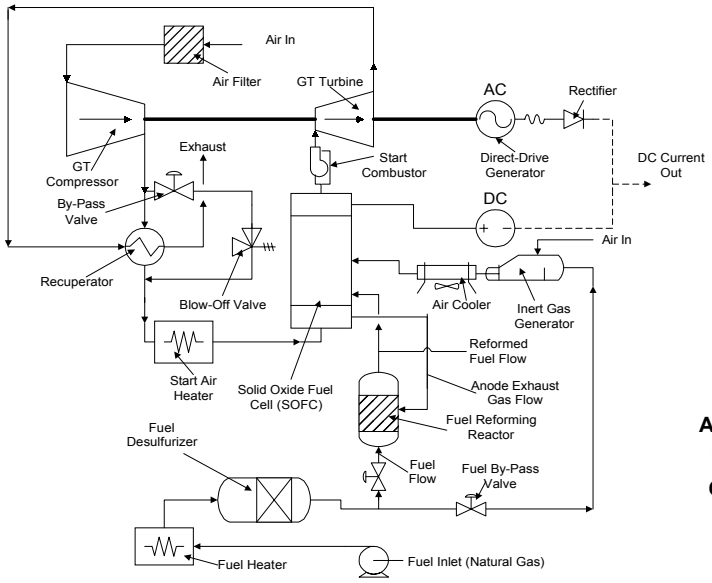

Figure 1. Generic hybrid solid oxide fuel cell gas turbine engine cycle based upon a recuperated gas turbine engine.

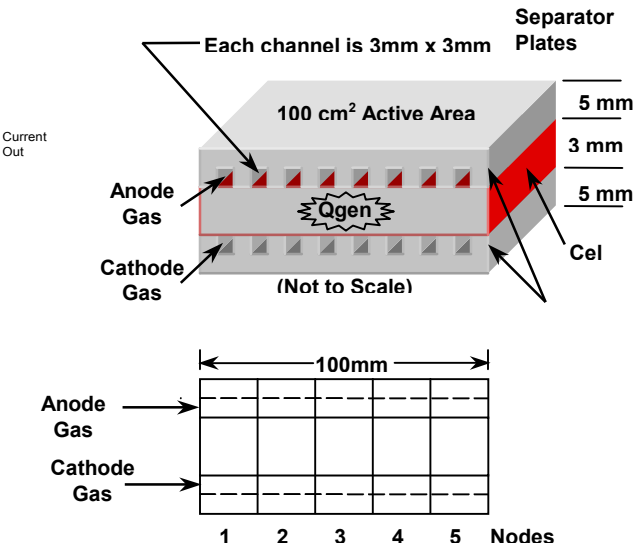

Figure 3. Schematic of molten carbonate fuel cell dynamic model geometry.

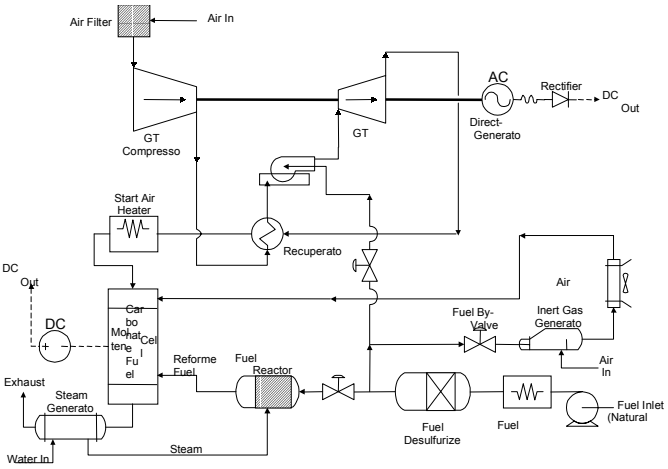

Figure 2. Generic hybrid molten carbonate fuel cell gas turbine engine cycle based upon a simple cycle gas turbine engine.

(a) cell voltage

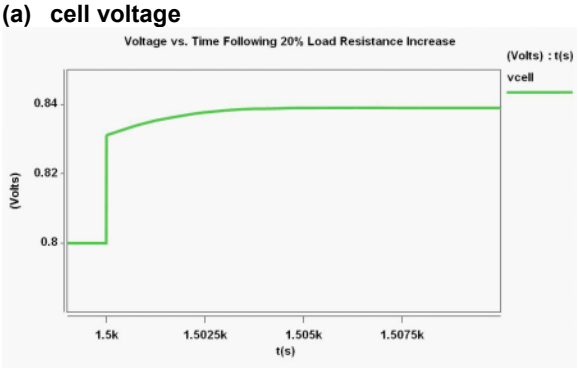

(b) current density

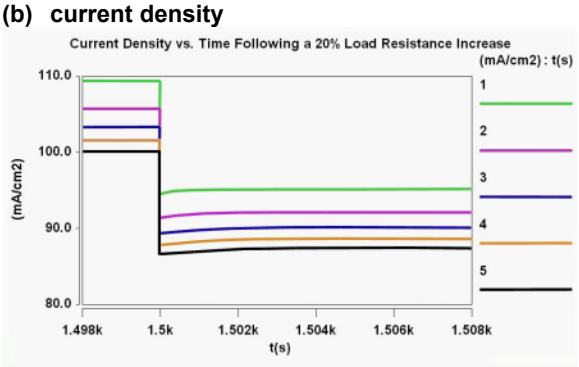

(c) loss distribution

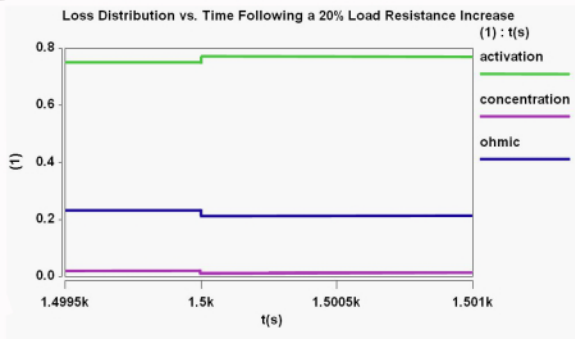

(d) hydrogen mole fraction

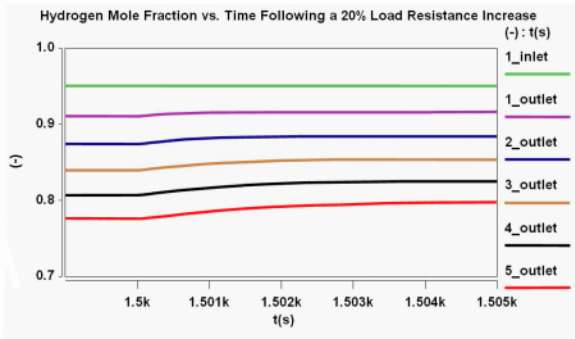

(e) anode gas temperature

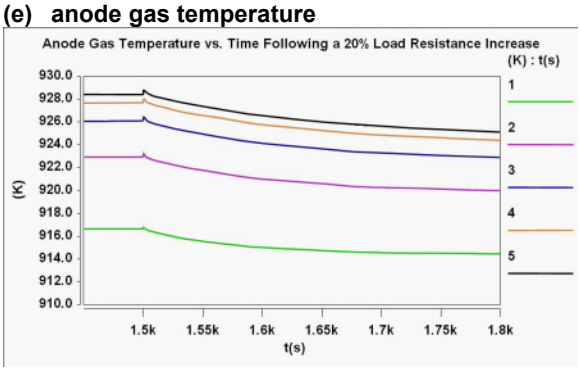

Figure 4. Response of molten carbonate fuel cell dynamic model to a 20% perturbation in load

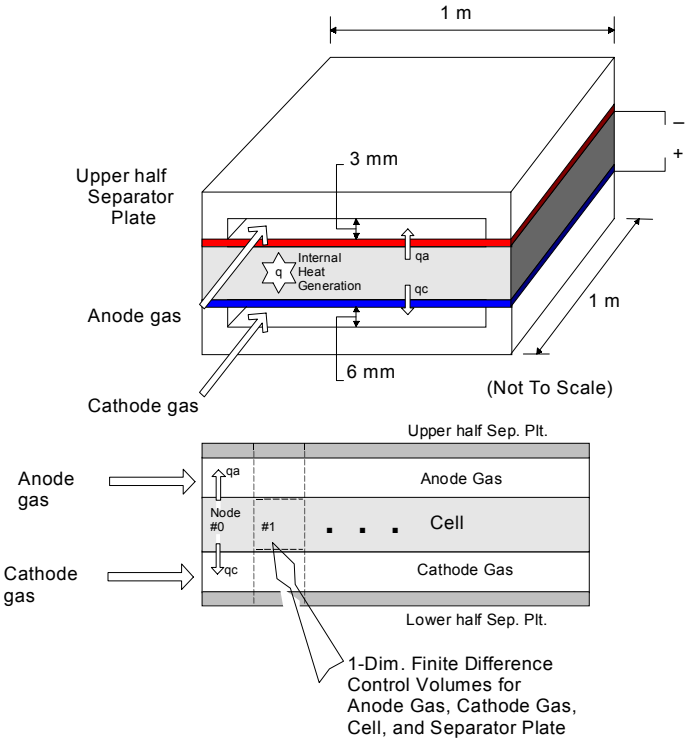

Figure 5. Generic planar solid oxide fuel cell design. Active area = 1 m^2.

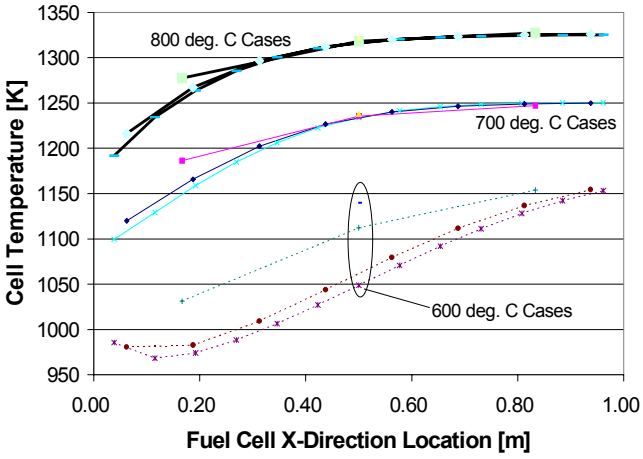

Figure 6. Steady-state cell temperature results for three different cathode supply temperatures, and using different number of nodes (1, 3, 8, 13).

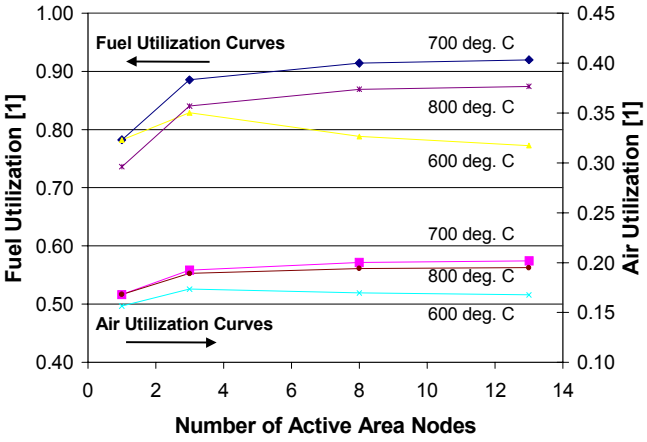

Figure 7. Steady-state fuel and air utilization results for same cases shown in Figure 6.

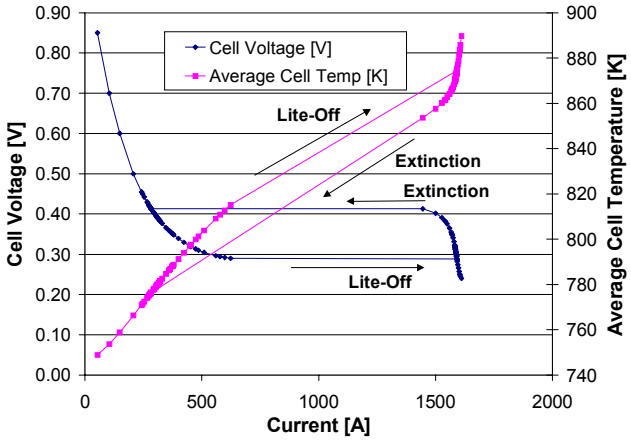

Figure 9. Fuel cell 'Lite-Off' and 'Extinction' curves.

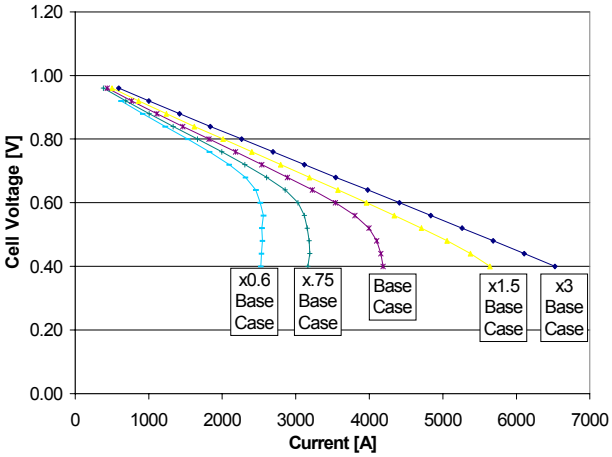

Figure 8. Steady-state cell voltage vs. current for several hydrogen flow rates. Designations show anode gas flow rates relative to base case of 0.022 g-mole/sec. Anode gas: 69% H_2 & 31% inert. Cathode gas: 95% O_2 & 5% inert. Oxygen utilization negligible for all cases.